*The Aeronautical Journal* (2023), **127**, pp. 193–212
doi:10.1017/aer.2022.71

**REGULAR PAPER**

# Role of flexibility on the aerodynamic performance of a resonating hummingbird-inspired wing

D. Kumar[1], G. Singh[2], P.M. Mohite[3], E.M. Lau[1,*] and Y.-C. Wang[1]

[1]Department of Aeronautical Engineering, Chaoyang University of Technology, Taichung, Taiwan, [2]Department of Aerospace Engineering, University of Michigan, Ann Arbor, USA and [3]Department of Aerospace Engineering, Indian Institute of Technology Kanpur, Kanpur, India
*Corresponding author. Email: edwin@cyut.edu.tw

**Received:** 10 November 2021; **Revised:** 13 April 2022; **Accepted:** 21 June 2022

**Keywords:** Flapping wing; Micro air vehicle; Fluid-structure interaction; Biomimicking; Wing flexibility; Resonant flapping

## Abstract

This work investigates the role of flexibility and resonant excitation on the deformation mechanism and aerodynamic performance of flapping wings. A hummingbird-inspired wing (HIW) is considered and designed to have a bone-like stiffener made of carbon fibre/epoxy (CF/E) composite attached to a membrane made of carbon nanotubes/polypropylene (CNTs/PP) nanocomposite representing the flexible part of the natural wing. The designed HIW model is analysed through fluid-structure interaction simulations performed at frequencies near and at resonant frequency. It is found that HIW generates desired bending and twisting deformations that are coupled. These deformation mechanisms are studied in detail with the help of time-varying deflections and bending-twisting angles. Further, the simultaneous effect of these parameters on the aerodynamic performance of the wing is also investigated. It is observed that the coupled nature of bending and twisting deformations is critical in enhancing the aerodynamic performance of flapping wings. In addition to that, the resonance generates higher amplitude of desired structural deformations that further enhances thrust as well as lift generation capability of the wing. The underlying mechanism for this is also explained by studying the flow around the deflected surface of the wing. Compared to off-resonant frequencies, vorticity and pressures are substantially higher for the wing at resonance. A physical model of HIW is realised using CNTs/PP and CF/E composites to perform experimental wing motion analysis and to validate the computational results. In conclusion, the present study provides a basis to design efficient biomimetic flapping wings for micro aerial vehicles (MAVs) by exploring flexibility and resonant excitation.

## Nomenclature

| | |
|---|---|
| $l$ | wing length |
| $c$ | mean chord |
| $a$ | heaving amplitude |
| $f$ | heaving excitation frequency |
| $f_n$ | resonant frequency |
| $U_0$ | reference velocity |
| $p$ | pressure |
| $Re$ | Reynolds number |
| $L$ | lift force |
| $T$ | thrust force |
| $C_L$ | coefficient of lift |
| $C_T$ | coefficient of thrust |
| $v$ | kinematic viscosity |
| $\eta_p$ | propulsive efficiency |
| $\delta$ | wing deflection |

| | |
|---|---|
| $\phi_b$ | wing bending angle |
| $\phi_t$ | wing twisting angle |
| $\rho_f$ | air density |

## 1.0 Introduction

Hummingbirds are the most agile natural flyers among birds. They are considered as one of the masters of flapping flight. From the species of flapping insects to gliding avians, hummingbirds abridge the two worlds of organisms. Throughout their evolution, they have established their habitat and feeding habits with their mechanism of flapping flight that enables highly abrupt, articulate and manoeuvrable motion. However, from the rich studies of their anatomy and behaviours, it seems that their way of flying demands considerable energy, so the wing motion must be highly efficient. Several studies have investigated natural hummingbird wings to study their aerodynamics and other characteristics during various flight modes including hovering. Warrick et al. [1] performed aerodynamic measurements where wake of a hovering rufous hummingbird was studied. The authors reported that hummingbirds produce 75% of their weight support during downstroke and remaining 25% during upstroke. It was also reported that hummingbirds, the only kind of bird that hovers, exploit insect-like aerodynamic mechanisms such as leading edge vortices (LEVs) at a Reynolds number (Re) of as low as Re = 3,000. Elimelech and Ellington [2] studied flow characteristics of a fixed hummingbird wing and reported a laminar to turbulent transition at Re value of 5,000 to 15,000. The aerodynamics of revolving natural and modelled hummingbird wings was studied by Altshuler et al. [3] where it was observed that the lift to drag ratio of natural wings is substantially higher due to morphological contributions of feathers. Krupt et al. [4] studied 26 different natural hummingbird wings in a revolving mode in hovering flight scenario and observed that the aspect ratio (AR) has a significant effect on the aerodynamic performance of the wings. The natural hummingbird wings also undergo complex flapping-pitching motion inducing bending and twisting deformations to generate the desired aerodynamic forces [5–7]. Maeda et al. [8] quantified dynamic wing morphing of a hovering hummingbird with the help of high-speed videography. The authors showed that the wing shape changes significantly during a flapping stroke. The authors also reported the presence of substantial span-wise bending along with camber and span-wise twisting in hummingbird wings. Tobalske et al. [9] studied three-dimensional kinematics of hummingbirds (Selasphorus rufus) in a wind tunnel and observed that their small size can significantly alter wing kinematics such as chord angle, wingbeat amplitude and angle-of-attack without changing wingbeat frequency during various flight manoeuvres including hovering and forward flight. Ingersoll and Lentink [10] showed that hummingbirds have evolved a mechanically efficient wingbeat with the help of elastic recoil phenomena that helps them to overcome the inertia of flapping wings. In 1960, Greenewalt [11] discovered that the natural flyers such as hummingbirds and insects flap their wings at nearly constant frequency during all flight operations. This particular frequency phenomena was called the characteristic frequency of flapping, or physically, resonant flapping. At this frequency, hummingbirds as well as insects generate maximum amplitude of wing motion, which enhances their aerodynamic efficiency. Realising the role of resonance, Jafferis et al. [12] and Zhang et al. [13] experimentally demonstrated an increase in efficiency at resonant excitation. Raney and Slominski [14] fabricated hummingbird-inspired wings using carbon fibre/epoxy (CF/E) composite as the stiffeners and latex as the membrane. They also developed a vibratory resonant mechanism using two electrodynamic shakers to study the deforming behaviour of the wings at their characteristic frequency. The authors were able to replicate the bird's complex wing motions, including reverse camber. The lift produced by reverse camber is supported by Ingersoll and Lentink [10]. Chen et al. [15] further suggested that the structural deformations of a flapping wing depend on the aerodynamic and inertial-elastic forces. Combes and Daniel [16] separated the inertial-elastic forces from aerodynamic forces by studying insect wings inside a vacuum chamber. The authors concluded that the contribution to wing deformation of aerodynamic forces is relatively small as compared to the inertial-elastic forces. Masoud and Alexeev [17] carried out extensive fluid-structure

https://doi.org/10.1017/aer.2022.71 Published online by Cambridge University Press

interaction (FSI) simulations on simple rectangular-planform wings that were excited at on and off their resonance frequencies. These flexible wings were set in an anhedral configuration and provided with a sinusoidal heaving motion at their root. The study revealed that resonant oscillations of large-amplitude significantly enhance the aerodynamic lift and efficiency. Also, at resonance, the aerodynamic forces of these simple thin plates of rectangular planform are comparable to that of small insects. The authors reported that these simple flexible wings excited with a resonant heaving motion are useful for developing efficient micro aerial vehicles (MAVs). The authors suggested that a significant thrust can also be derived by optimising the stiffness distribution in the wing. Tobing et al. [18] performed FSI simulations on bumblebee-inspired wings of rigid to varying span-wise flexibility. It was realised that flexibility prevented the early separation of leading edge vortices (LEVs), which in turn increased the lift of the wing. Young et al. [19] demonstrated that attached flow could be maintained by controlling the time-varying wing twist and camber. Their flexible wings were able to generate thrust for a forward flight, while rigid wings produced drag. However, a rigid wing happened to have a high power economy in contrast to the flexible ones. Interestingly, at flexibility close to a natural wing structure, the wing becomes less efficient than other wings of uniform stiffness. Thus, the authors proposed that wing stiffness variation should be based on real material properties of the wing elements, and stiffness distributions must be optimised for better performance. Meanwhile, Frampton et al. [20] reported that the phase between bending and torsional deformations of a resonating wing is critical to the production of thrust. Various studies concluded that both span-wise and chord-wise flexibility play an important role for optimising the aerodynamic performance of a flapping wing structure [21–29]. Senda et al. [30] found that flexibility not only enhances aerodynamic efficiency but also improves flight stability through passive wing torsion.

Despite over two decades of extensive research, there is still no sufficiently efficient MAV able to carry out prolonged operations. One of the key reasons is that many MAVs are not implemented with optimum wing flexibility. It is well understood that taking inspiration from hummingbirds could help in achieving a wing design with desired order and arrangement of flexibility. In addition to that, while exploring the deformations of a flexible wing at resonance, there has yet to be an investigation on the underlying FSI mechanisms that lead to the improvement of aerodynamic performance of hummingbird-like wings at resonant excitation. In the present study, a hummingbird-inspired wing (HIW) model is used to investigate the combined role of flexibility and resonant excitation on its aerodynamic performance. In terms of structural configuration, the HIW model consists of bone-like stiffener made of carbon fibre/epoxy (CF/E) composite at the leading edge which is attached to carbon nanotubes/polypropylene (CNTs/PP) nanocomposite membrane representing the flexible part of the natural wing. A set of coupled FSI simulations are carried out on the HIW model to obtain its deformation mechanisms and aerodynamic forces as a result of the heaving excitation at the root. The study is divided into two parts. In the first part, the flexibility of HIW model is analysed by exciting it at its characteristic frequency. The model is basically evaluated on the basis of its efficacy in generating desired bending-twisting deformations for enhanced aerodynamic performance. In the second part of this study, the wing is analysed at frequencies in the neighbourhood of the fundamental mode resonant frequency of the wing to investigate the role of resonance. For experiments, the CNTs/PP nanocomposite is fabricated and used with the CF/E composite material for fabricating the physical model of the HIW model for experimental wing motion analysis and validating the computational results. A heaving mechanism is fabricated to excite the wings. The measurement of wing motion is carried out using an in-house 3D digital image correlation (DIC) technique.

## 2.0 Materials and methods

In this section, a description of the developed wing design is presented. The study of the wing design is primarily performed through FSI simulations and is supported via experimental measurement of the deflections. The setups of numerical simulations and experiments are presented here in detail.

https://doi.org/10.1017/aer.2022.71 Published online by Cambridge University Press

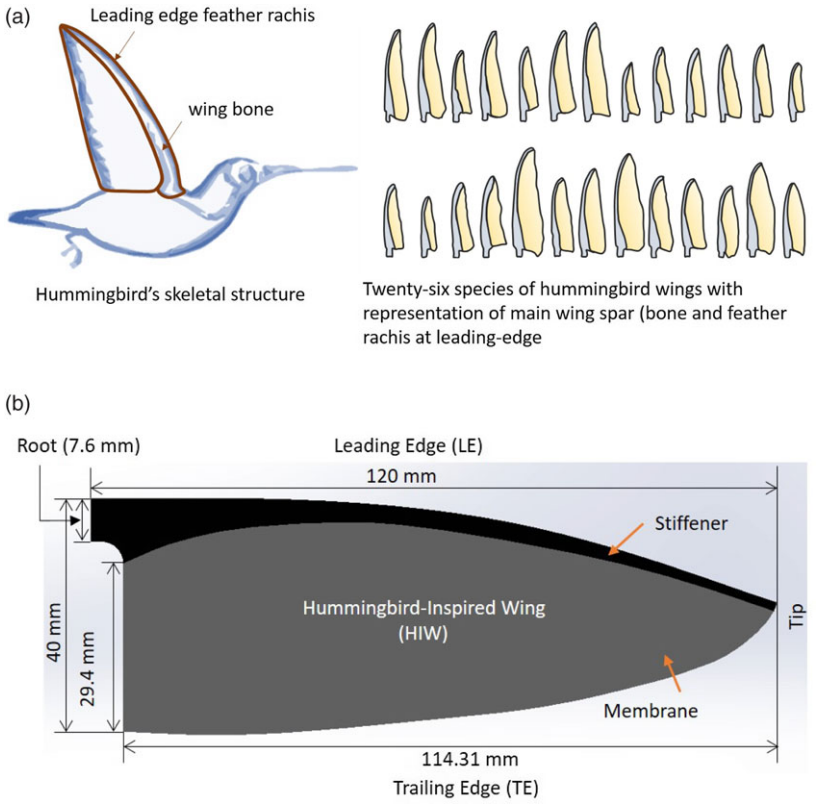


***Figure 1.*** *(a) Bioinspiration: Hummingbird and its wings, reproduced from Refs [4,34], (b) hummingbird-inspired wing (HIW).*

### *2.1 Designing of the bioinspired wing*

From the inspiration of hummingbird flights, the present study utilises a design simplified but with the inclusion of basic geometric and structural features of a natural hummingbird. This hummingbird-inspired wing (HIW) model consists of a stiffener at the leading edge which is attached to a flexible membrane that serves as the planform surface. Composite materials have been utilised to design a realistic wing and mimic the natural hummingbird wing structure. It has been observed that the CNTs/PP nanocomposite is a suitable material to mimic natural flapping wings for MAVs [31,32]. Here, the CNTs/PP nanocomposite material is chosen to represent the flexible part of the natural hummingbird wings, which comes due to feathers. The main load-bearing component of a feather is rachis. The reasons for selecting CNTs/PP nanocomposite are two folds, one is the matching of mechanical properties towards biomimicking and another is based on establishing multifunctionality in the wings. We have compared the fundamental mechanical properties of the selected material with the structural members, i.e. feather rachis of natural wings. We found that the storage modulus or elastic modulus of the nanocomposite is close to that of the natural counterpart [33]. This is useful in achieving true biomimicking in the wings. Apart from that, PP is a light, flexible and fatigue resistant polymeric material which are essential characteristics for flapping wings, as natural wing materials are evolved to have such characteristics. On the other hand, CF/E-based composites are the mostly used stiffener materials for flapping wings. This is due to their good stiffness-to-weight ratio. In the HIW model, CF/E composite is used as the stiffener that also represents the bone and leading edge feather rachis of the natural wing (see Fig. 1(a)). Moreover, the design of the wing is achieved in such a manner that it would help to replicate the deformation behaviour of the natural wings and understand its potential for the realisation of realistic

https://doi.org/10.1017/aer.2022.71 Published online by Cambridge University Press

physical prototype. A schematic of the HIW model is shown in Fig. 1(b). The overall dimensions of the wing are: wingspan 120mm, chord 40mm (maximum), and thickness 0.3mm. The wing is excited with a sinusoidal heaving motion provided at its root/base in both experimental and computational studies. The reason behind selecting the heaving excitation is to design an efficient bioinspired wing that would perform efficiently even with a simple one-dimensional input excitation. The frequency of the chosen heaving excitation is obtained using Equation (1) discovered by Greenewalt [11]. This empirical relation between the characteristic frequency and wing length is considered as the basis for the wing flexibility analysis. The wing is excited with a heaving frequency of 14.38Hz that is based on the wing length of 120mm (see Fig. 1). For resonance analysis, the simulations are also performed at off and on resonant frequencies of HIW model. In the resonant excitation analysis, the excitation frequencies are normalised with respect to the first fundamental mode resonant frequency of the wing model. The amplitude of given sinusoidal heaving is maintained at 5% of the wing length. The wind velocity is set at 0m/s in all the simulations, considering the hovering flight scenario.

$$f \times l^{1.15} \cong 3540 \tag{1}$$

where, $f$ is the beat-rate or characteristic frequency (Hz), and $l$ is the wing length (mm).

### *2.2 Computational method*

The computational simulations are performed using ANSYS System Coupling module, which couples and controls the Transient Structural (structural solver) and Fluent (flow solver) modules for carrying out the two-way FSI simulations. The structural solver considers the geometric and material non-linearity to model the flexibility of the wing. The flow solver has a moving mesh and remeshing scheme to adapt to the moving FSI interface boundary. The goal of performing strongly coupled FSI studies is to determine the structural deformations and aerodynamic forces generated by the wing under dynamic excitation. Figure 2 illustrates the details of the computational fluid dynamics (CFD) domain for fluid dynamic simulation part of FSI, meshing of the wings for structural dynamic simulation part of FSI, and input motion provided at the root of the wings. The heaving motion given to the wing is generated in the structural solver using the displacement-controlled boundary condition. The coupling between the structural and flow solvers occurs through the wing surface as the interface.

#### *2.2.1 Structural dynamic model*

In the Transient Structural solver, the non-linear equation of motion for the solid medium is solved using an implicit time integration scheme. The CAD model of the HIW is generated using ANSYS Design Modeler. The wing model is then meshed using the ANSYS Meshing tool. The total number of elements for the model are 10,299. The meshing of the wing model is basically carried out with SOLID 187 elements (10-node 3D tetrahedral structural solid). The meshed model of HIW is also shown in Fig. 2. The material inputs for the stiffener and the membrane are unidirectional CF/E composite and CNTs/PP nanocomposite, respectively. In other studies, we developed CNTs/PP nanocomposites and characterised them for static mechanical properties [35] and dynamic mechanical properties [31]. The studies showed that 0.1 weight percentage addition of multi-walled CNTs gives the highest elastic modulus and strength values in comparison to other weight percentage cases (0–1wt%). Therefore, in the present study, the 0.1wt% CNTs/PP nanocomposite's density, Young's modulus and Poisson's ratio are taken, i.e. 904kg/m$^3$, 1.31GPa, and 0.45, respectively. The input material data for the unidirectional CF/E composite sheet is given in Table 1.

#### *2.2.2 Fluid dynamic model*

ANSYS Fluent module is used to perform the fluid dynamic part of the FSI simulations. Dynamic meshing is used to handle the wing motion during CFD analysis. The SIMPLEC method is employed for solving the Navier-Stokes equations. A cubic domain is created around the wing (refer to Fig. 2).

https://doi.org/10.1017/aer.2022.71 Published online by Cambridge University Press

***Table 1.*** *Mechanical properties of CF/E composite, where, $\rho$ is density; $E_{11}$, $E_{22}$, $E_{33}$ are elastic moduli in x, y and z directions, respectively; $G_{12}$, $G_{13}$ and $G_{23}$ are shear moduli in xy, yz and xz planes, respectively; $\nu_{12}$, $\nu_{13}$ and $\nu_{23}$ are Poisson's ratios in xy, yz and xz planes, respectively*

| Property | $\rho$ | $E_{11}$ | $E_{22}$ | $E_{33}$ | $G_{12}$ | $G_{23}$ | $G_{31}$ | $\nu_{12}$ | $\nu_{23}$ | $\nu_{31}$ |
|---|---|---|---|---|---|---|---|---|---|---|
| Value | 1,490 | 121 | 8.6 | 8.6 | 4.7 | 3.1 | 4.7 | 0.27 | 0.4 | 0.27 |
| Unit | Kg/m$^3$ | GPa | GPa | GPa | GPa | GPa | GPa | – | – | – |

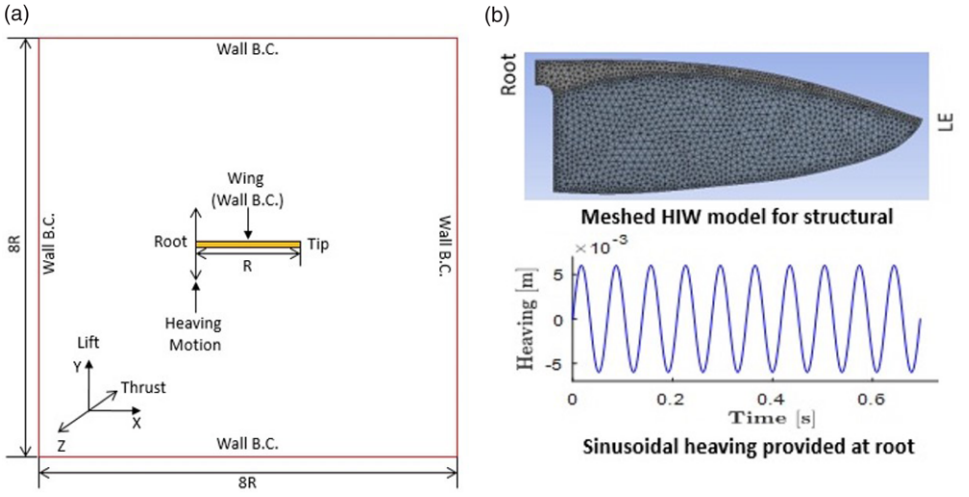


***Figure 2.*** *Description of CFD domain, meshed model of the wings, and the input motion (drawings – not to scale). Lift is a positive force in the vertical direction same as the heaving excitation. Thrust is the horizontal force opposite to drag along the root of the wing (negative value of drag).*

The meshing of the CFD domain is done with tetrahedral cells using patch conforming method. The boundary conditions are set with a velocity of 0.0m/s, an outlet pressure of 0.0Pa, the domain sides and wing surfaces obey the no-slip condition (wall boundary condition (B.C.)). For symmetry, only one wing is simulated in the FSI domain. The time-varying coefficients of lift and thrust are obtained as $C_L = 2L/\rho_f U_0^2 cl$, $C_T = 2T/\rho_f U_0^2 cl$, respectively, where $L$ is time-varying lift, $T$ is time-varying thrust, $\rho_f$ is the air density, $c$ is the mean chord and $l$ is the wing length [17,18]. The reference velocity used for calculating the coefficient depends on the heaving amplitude and it is defined as $U_0 = 2\pi af$, where $a$ is the heaving excitation amplitude and $f$ is the heaving frequency. The range of Reynolds number ($Re$) investigated in this study is $Re = 932$ to 1,863, which is defined as $Re = 2\pi fac/\nu$, where $\nu$ is the kinematic viscosity [17]. Hummingbirds and insects flap their wings at a very high amplitude. Masoud and Alexeev [17] performed their FSI simulations by exciting a simple rectangular flapping wing at a heaving amplitude of $0.2l$ (20% of the wing length). Considering this level of excitation amplitude in the present study, the value of Re at resonance comes out to be 5,217, which lies in the range of 5,000–30,000 (a typical Re range for hummingbirds). However, the present study saw FSI simulations fail due to extremely high amplitude deflections of the flexible wing at resonance. Therefore, the amplitude of input heaving excitation is reduced to 5% of the wing length ($a = 0.05 \times l$), which corresponds to a Re value of 1,304 at the resonant frequency, i.e. 14Hz. In addition, various studies have reported that the hummingbirds during hovering exploit high-lift aerodynamic mechanisms such as LEVs like insects. One of the main reasons is the presence of extremely low Re flow for both kinds of flyers as suggested by Warrick et al. [1] and Song et al. [36].

https://doi.org/10.1017/aer.2022.71 Published online by Cambridge University Press

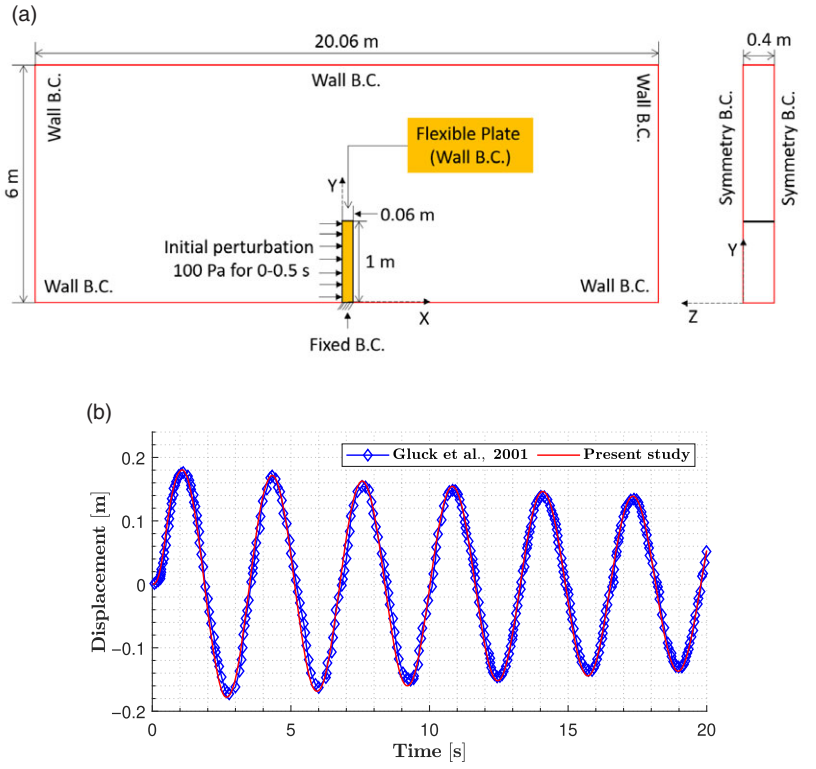


***Figure 3.*** *(a) Description of the validation case (not to scale, B.C. stands for boundary condition), (b) comparison of oscillation displacements for 20s.*

*2.2.3 Validation of FSI method*

The validation of the used FSI method is carried out by simulating the oscillations of a thin flexible plate in a resting fluid. This benchmark FSI problem is considered from the work carried out by Gluck et al. [37]. This problem has also been investigated in other studies [38–40] for validating FSI methods and studies. The dimensions of the plate and the fluid domain, along with the associated boundary conditions, are illustrated in Fig. 3(a). The properties of the plate's material and the surrounding fluid are given in Table 2. Meshing of the flexible plate is carried out using 1,080 solid elements (SOLID 186), whereas 200,000 Hexahedral cells are used for the fluid domain. This 3D simulation is performed for 20s with a time step of 0.0125s. An initial perturbation pressure of 100Pa is applied on the -X side of the plate from the start till 0.5s. These simulation parameters were suggested in the validation study performed by Chimakurthi et al. [38]. The comparison of the results is based on the displacement of the free end of the plate, as shown in Fig. 3(b). The present results clearly show the presence of damped oscillating behaviour of the plate. The oscillation displacements from the present study are in good agreement with the ones from Gluck et al. [37]. This validates that the FSI approach used in the present study is able to perform 3D coupled simulations for a flexible dynamic structure.

*2.2.4 Sensitivity analysis*

The sensitivity studies performed in this work are associated with the number of heaving cycles as well as the size of and the level of discretisation of the fluid domain. Figure 4 shows the sensitivity study results, the first study considers two mesh sizes for the fluid domain, baseline with 266,670 cells and fine with 440,812 cells. The domain size for this case is 8 times the length of the wing. Also, for this case,

https://doi.org/10.1017/aer.2022.71 Published online by Cambridge University Press

***Table 2.*** *Oscillating plate's material and surrounding fluid properties*

| Matter | Properties | | |
|---|---|---|---|
| Plate material | Elastic modulus (GPa) | Poisson's ratio | Density (kg/m$^3$) |
| | 0.0025 | 0.35 | 2,550 |
| Fluid domain | Dynamic viscosity (Pa-s) | Density (kg/m$^3$) | Flow velocity (m/s) |
| | 0.2 | 1 | 0 |

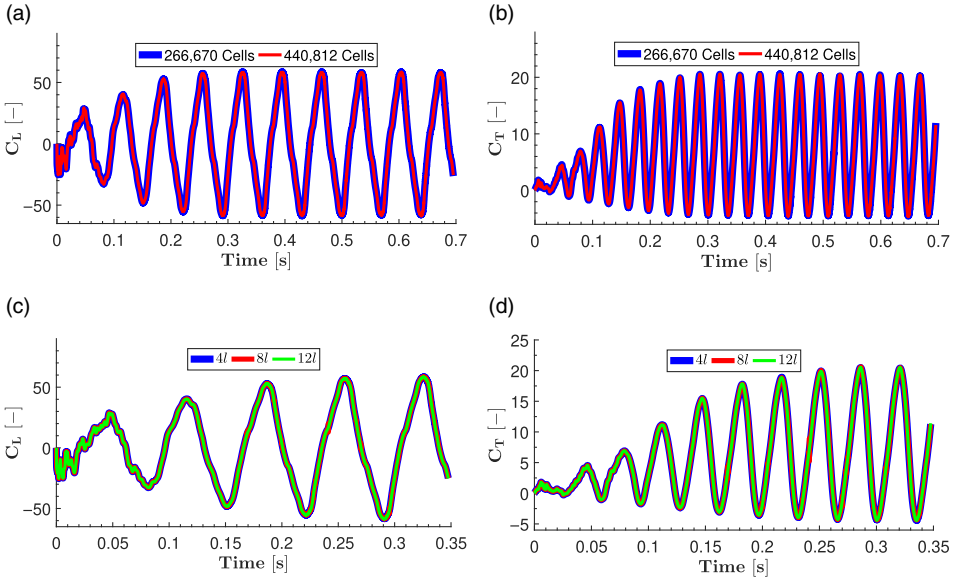


***Figure 4.*** *(a) Mesh independence of $C_L$, (b) mesh independence of $C_T$, (c) domain size independence of $C_L$, (d) domain size independence of $C_T$.*

the FSI simulations are performed over 10 cycles. This is to identify the number of cycles it takes before steady state is reached. The baseline and fine mesh models produce similar results. Also, the solution reaches the steady state after fifth cycle of the excitation. Finally, in Fig. 4(c) and (d), three domain sizes, 4$l$, 8$l$ and 12$l$ are considered ($l$ is the wing length). As it can be seen that the results are similar for all three domain sizes. Thus, the FSI simulation in further studies are performed over 10 heaving cycles with a domain size of 8$l$ and the baseline mesh size of 266,670 cells.

### *2.3 Experimental methods*

In the present study, we have performed experimental validation of the structural dynamic results from the FSI simulations. The objective was to compare the experimental resonance frequency and corresponding structural deformations with the ones from computational FSI simulations. In that direction, the physical model of HIW is fabricated. A unidirectional CF/E sheet is cut to form the stiffener of the HIW. The CNTs/PP nanocomposite films are fabricated using a solvent casting method. The CF/E composite stiffener and CNTs/PP nanocomposite membrane are attached together to form the entire wing.

For the purpose of excitation during the experimental measurements, a heaving mechanism is developed which can provide simple sinusoidal heaving motion to the fabricated wing model. This mechanism basically converts the circular motion of a DC motor to linear heaving motion. Figure 5 illustrates the CAD model of the complete wing testing model consisting of two wings, heaving mechanism and a DC

https://doi.org/10.1017/aer.2022.71 Published online by Cambridge University Press

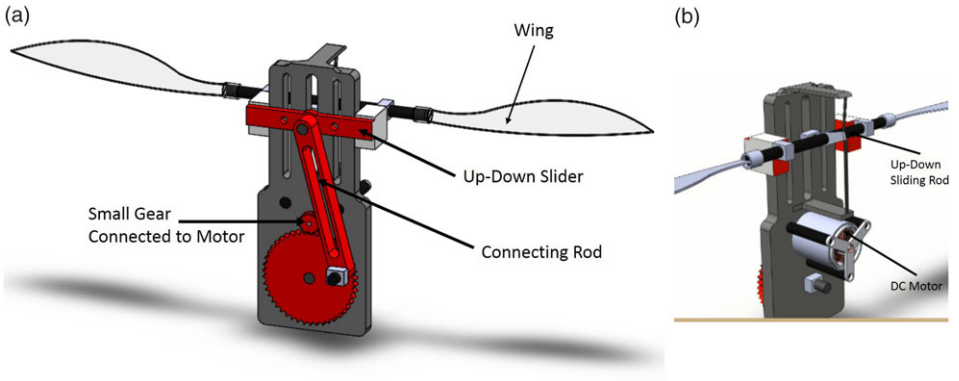


***Figure 5.*** *CAD model of the fabricated wing testing model, (a) front side of the model showing heaving mechanism and wings, (b) back side of the model showing DC motor and supporting elements.*


***Figure 6.*** *The fabricated model of the hummingbird-inspired wing (HIW).*

motor along with chassis and supporting elements. All the intricate and complicated parts of the mechanism are cut out from a 2mm thick acrylic (PMMA) sheet using laser machining. Small supporting rods used for attaching motor, wings and other elements are fabricated using hollow CF/E composite tubes. The DC motor is controlled using an electronic speed controller (ESC), which provides power and pulse-width modulation (PWM) signal to the motor. The duty cycle of a PWM pulse, the ratio of time for which it is high and low, determines the RPM of the motor. An Arduino microcontroller is used to generate the signal at pre-defined time steps. It requires the heaving frequency input from the user. This is the frequency in Hz at which the heaving excitation is required for the experiment and/or possible flight in future. The program initiates with calibrating the ESC. This is followed by the Rise Time. The mechanism begin to excite at 1Hz irrespective of the required frequency and is smoothly increased to the required frequency.

An in-house 3D digital image correlation (DIC)-based non-contact measurement method is used for the motion measurement and structural dynamic analysis of the wings [41]. It consists of two high-speed cameras (Olympus i-Speed TR), a NI cRIO 9076 real-time FPGA-based (RT-FPGA) operating system, data acquisition modules, a workstation, and a laser displacement sensor. The high-speed cameras record images of the wings painted with black and white speckles. The high-speed cameras are synchronised with the laser displacement sensor using RT-FPGA system. The recorded images are correlated to obtain the displacements of the wings under the heaving motion driven by the mechanism. A modal shaker (B&K Type 4808) is used for performing the modal testing of the wing. The fundamental natural frequencies of the wings are obtained by performing the fast Fourier transform of the wing-tip displacement data measured using laser displacement sensor. The structural deforming shape at first fundamental natural frequency ($f_n$) is obtained by full-field mapping of DIC displacement data. The fabricated wing and the experimental setup are shown in Figs 6 and 7, respectively.

https://doi.org/10.1017/aer.2022.71 Published online by Cambridge University Press

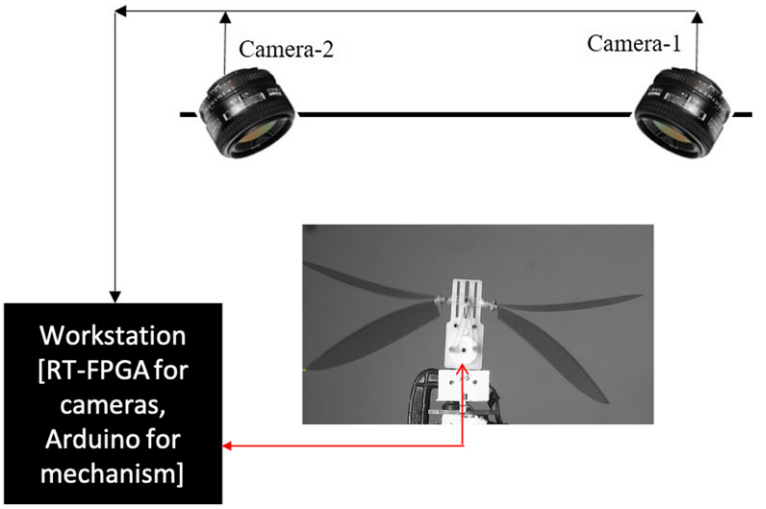


***Figure 7.*** *DIC-FPGA-based measurement setup and heaving mechanism for wing testing [41].*

## 3.0 Results and discussion

Wing deformations and aerodynamic parameters are computationally evaluated and analysed using ANSYS FSI solver. Experimentally, the wing is excited with the heaving mechanism and its deformations are measured using DIC technique. Here, wing flexibility analysis is investigated first, which is followed by resonance analysis. The performance of the wing is evaluated by examining the structural deformations along with aerodynamic forces and flow characteristics. The experimentally obtained natural frequencies and deformations are compared with the computational results at the end.

### *3.1 Role of the wing flexibility*

To understand the role of flexibility, we have performed a detailed analysis of structural deformation mechanisms as well as the aerodynamic characteristics for the wing considered in the present study. During the FSI simulations for flexibility analysis, the HIW model is excited at the characteristic frequency obtained using the Greenewalt relation given by Equation (1) (leading to the heaving excitation frequency of 14.38Hz based on the wing length of 120mm). The deformed wing shapes and the comparison of deflections at the wing tip and at the root of the trailing edge, marked *rte*, are presented in Fig. 8. It can be seen that the HIW model generates coupled bending-twisting deformations. The comparison of the rte deflections clearly indicates that HIW has a substantial twisting deformation throughout the wing except the root where heaving excitation (Exc) is provided (see Fig. 8(c)).

The quantitative study of the structural deformations for the considered wing design is carried out via bending and twist angles over the excitation cycle as shown in Fig. 9. The bending and twisting angles are defined as the angle made by a wing element in *xy* and *yz* planes, respectively. We evaluated these angles at two key locations, one at the wing tip and second at the *rte*. HIW is able to produce coupled rotations both from tip to root, which results in a superior aerodynamic performance of this design. Further correlations of these deformations to the aerodynamics performance parameters are discussed in the following sections via flow visualisations at key instances.

Considering the aerodynamic performance, as the biomimetic wing model, i.e. HIW, generates large amplitude bending-twisting deflections, the lift and thrust forces generated by this model is of significant magnitude (see Fig. 10(b)). However, the average lift is zero due to symmetric heaving excitation.

https://doi.org/10.1017/aer.2022.71 Published online by Cambridge University Press

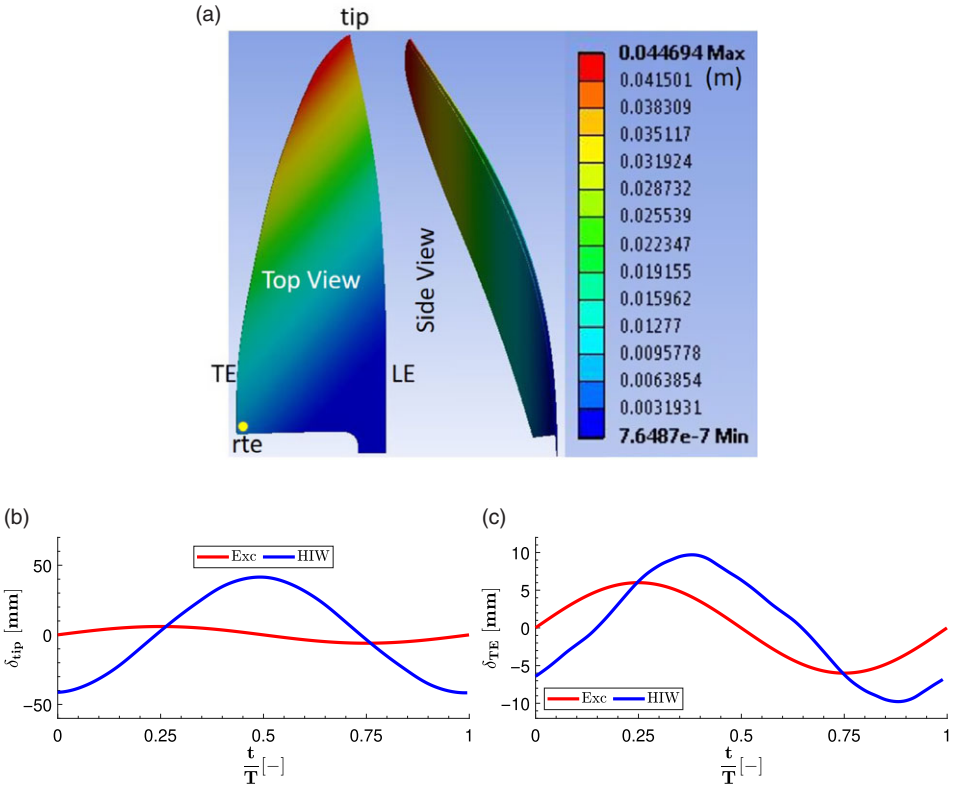


***Figure 8.*** *Structural deformation and deflections of HIW model at the characteristic frequency (Exc indicates the input motion provided at the wing root), (a) structural deforming shape of the wing, (b) comparison of deflections at the wing-tip with the input motion, (c) comparison of deflections at the trailing edge (at point rte) with the input motion.*

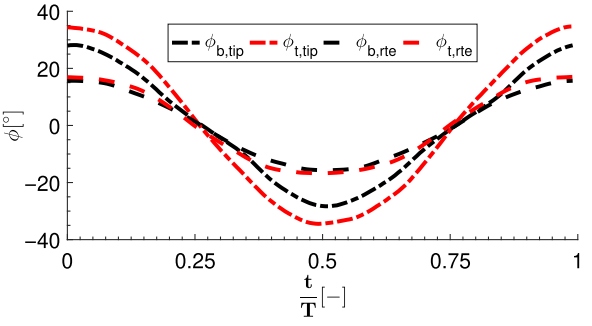


***Figure 9.*** *Bending and twisting analysis of HIW model at the characteristic frequency.*

The advantage of the HIW is demonstrated in terms of thrust. The presence of non-zero thrust can be attributed to the twisting of the wing. Table 3 presents the average and maximum aerodynamic force coefficients along with the propulsive efficiency ($\eta_p$) produced by the wing. The HIW model shows a very large magnitude of the thrust and that can be attributed to its adequate root flexibility as well as the large extent of bending-twisting coupling in the overall wing deformation under heaving motion. The extent of the bending-twisting coupling plays an important role in inducing an angle-of-attack to

https://doi.org/10.1017/aer.2022.71 Published online by Cambridge University Press

***Table 3.*** *Aerodynamic performance of HIW model at the characteristic frequency*

| mean $C_L$ | max $C_L$ | mean $C_T$ | max $C_T$ | $\eta_p$ |
|---|---|---|---|---|
| −0.01 | 58.51 | 7.8 | 20.60 | 0.0738 |

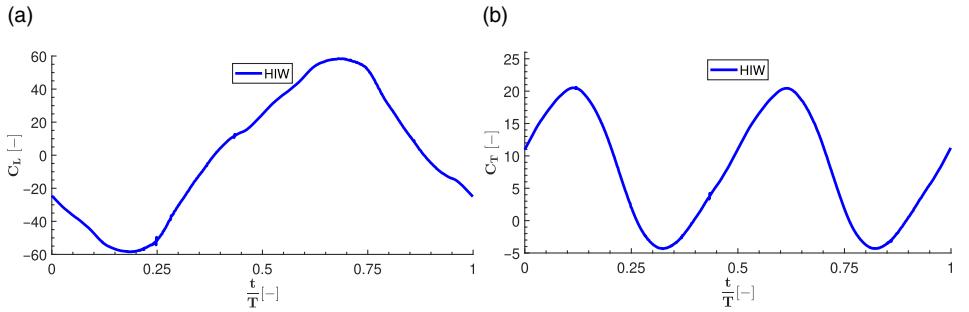


***Figure 10.*** *Aerodynamic forces generated by HIW model at the characteristic frequency, (a) $C_L$, (b) $C_T$.*

the ambient air in the heaving motion. The curvature in the stiffener (bio-mimicking bone structure of a hummingbird at the leading edge) as in the HIW exhibits significantly more bending-twisting coupling and flexibility along the span. These results indicate that the bending-twisting deformations play a key role in the aerodynamic performance of a wing. Proper placement of stiffeners or aeroelastic tailoring can indeed help in designing an aerodynamically efficient flapping wing structure. These insights are inline with the understanding from previous studies in literature [20,28]. The insights obtained from the investigations of the bioinspired wings can be translated towards enhanced performance of flapping wing based MAV designs.

### *3.2 Role of resonant excitation*

The flexibility analysis is further extended by performing the coupled FSI simulations at off and on resonant frequencies. Figure 11 shows the results of HIW including aerodynamic coefficients and propulsive efficiency as well as maximum deflections with respect to frequency ratio, i.e. the ratio of frequency in FSI (excitation frequency in air, $f_{\text{FSI}}$) to the first fundamental mode structural natural frequency (natural frequency without air, $f_{\text{structure}}$) of the wing model. The estimation of $f_{\text{structure}}$ for designed flexible wing is carried out by performing finite element modal analysis using ANSYS Modal module. The value of $f_{\text{structure}}$ for HIW model is 14.69Hz.

From Fig. 11, both the average and the maximum values of the lift as well as thrust coefficients peak near $\frac{f_{\text{FSI}}}{f_{\text{structure}}} = 1.0$. Consequently, the wing achieves the maximum propulsive efficiency just below its resonant frequency. This can be attributed to the peak deflections of the wing while under going resonant fluid-structure interactions. It can be inferred that the HIW model is able to yield its best aerodynamic performance due to the presence of peak coupled bending-twisting deformations achieved at $f_{\text{FSI}}$ which is slightly lower than $f_{\text{structure}}$. Among the frequency cases studied for HIW, the maximum deflections and aerodynamic forces occur at 14Hz which can be referred as the optimal frequency of flight for the wing. Interestingly, this optimal frequency is very close to the structural natural frequency ($f_{\text{structure}}$), i.e. 14.69Hz, which is a different scenario as compared to other similar studies. It should be noted that the present wing was under a simple heaving excitation, unlike the other studies where a rotating flapping motion was used. It has been observed in the literature that the resonant or characteristic flapping frequency of natural wings is significantly lower than their fundamental mode resonant frequency. The frequency ratio which is generally defined as the ratio of flapping frequency to the fundamental mode

https://doi.org/10.1017/aer.2022.71 Published online by Cambridge University Press

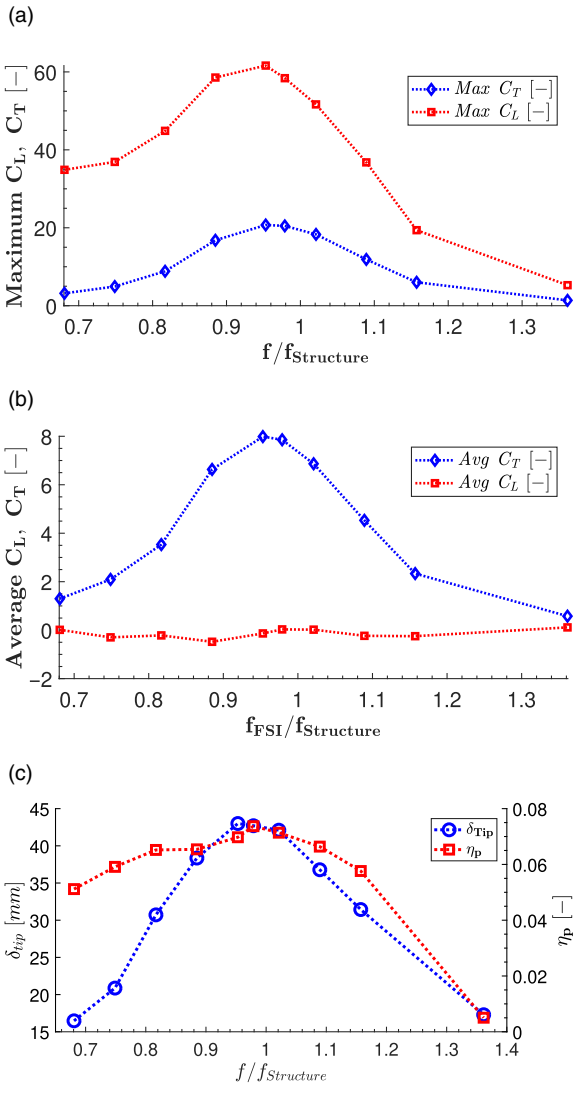


***Figure 11.*** *Aerodynamic forces and performance of HIW model on and off resonant frequencies, (a) maximum $C_L$ and $C_T$, (b) average $C_L$ and $C_T$, (c) propulsive efficiency and maximum deflection at the tip.*

frequency is in the range 0.2–0.3 for dragonflies [15] and hawkmoths [42]. Similar results have been reported in other studies [43–47]. The main reason behind this is the consideration of the same definition of the frequency ratio. However, in the present study, the frequency ratio is defined as the ratio of heaving excitation frequency to the fundamental mode structural resonant frequency. The wing acquires the highest amplitude of bending-twisting deformations (explained in following sections) when it is close to the fundamental resonant frequency which consequently enhances the aerodynamic performance of the wing. A similar observation has been reported in Masoud and Alexeev [17] as this study also considered similar excitation mode and definition of frequency ratio for a simple rectangular-shaped flexible wings. It can also be seen that the magnitude of the maximum of $C_L$ as well as $C_T$ is very high and become unusually large as the excitation approaches the resonant frequency. The reason behind this is the large deflections generated by the wing as compared to the amplitude of input heaving excitation. It

https://doi.org/10.1017/aer.2022.71 Published online by Cambridge University Press

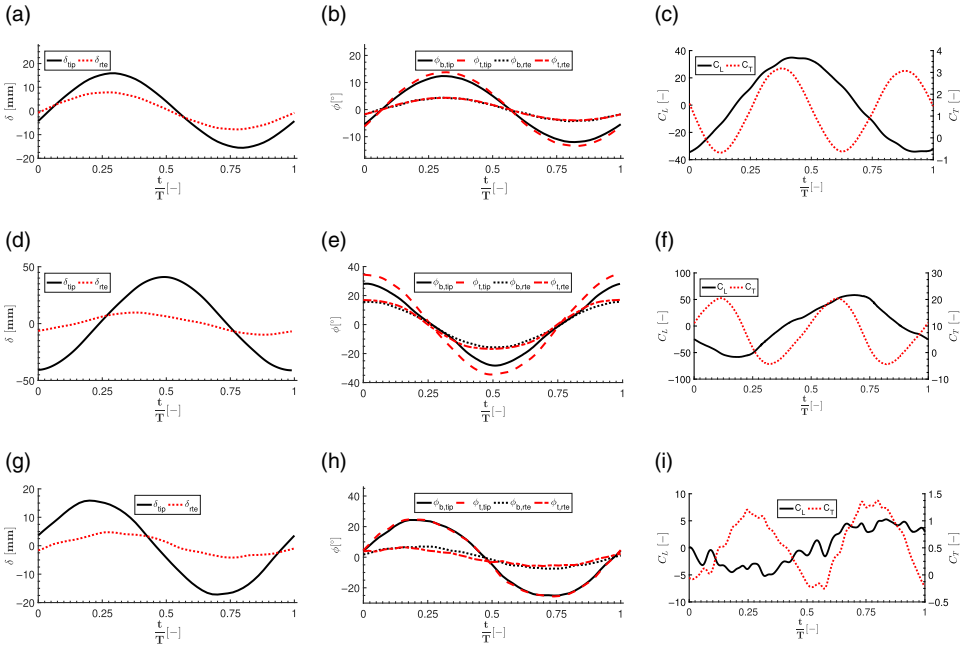


***Figure 12.*** *Structural deformations and aerodynamic forces on and off resonant frequencies, (a, b, c) 10Hz, (d, e, f) 14Hz, and (g, h, i) 20Hz.*

is important to note that the magnitude of the average of $C_L$ and $C_T$ consistently explain the physics of the problems considered in the present study.

### *3.3 Structural deformations vs aerodynamic forces*

Continuing the investigation of the role of flexibility at and off $f_n$, we discuss the wing deformation parameters along with output aerodynamic forces of the HIW. From the time histories of $\delta$, $\phi$, $C_T$ and $C_L$, through point *rte* to *tip* (see Fig. 12). It can be seen that $\delta_{\text{tip}}$ and $\delta_{\text{rte}}$, as well as $\phi_{b,\text{tip}}$, $\phi_{b,\text{rte}}$, $\phi_{t,\text{tip}}$ and $\phi_{t,\text{rte}}$ are generally higher at 14Hz as compared to the 10 and 20Hz cases. At the same time, both $C_L$ and $C_T$ are also high at 14Hz excitation. Off the resonance frequency at 10 and 20Hz, angles in bending $\phi_{b,\text{rte}}$ and twisting $\phi_{t,\text{rte}}$ at *rte* are very small in comparison to the *tip*, $\phi_{b,\text{tip}}$ and $\phi_{t,\text{tip}}$, respectively. Considering tip deflections for given sinusoidal heaving excitation (refer to the input excitation shown in Fig. 8), the tip deflection starts to lag (-ve out-of-phase) and reaches the maximum at 14Hz and starts decreasing and leads again at 20Hz. However, deflections at *rte* are almost in phase with input for all three cases. Additionally, for 10 and 20Hz, the bending and twisting angles are in phase with tip and root deflections. On the other hand, bending and twisting angles are almost opposite to tip deflections at 14Hz. Overall, when heaving cycle starts at $\frac{t}{T} = 0.0$ under resonance, the wing-tip is at the lowest position and lagging the input. It starts to move and pushes the air (due to positive bending and twisting angles) while following the input motion. Hence, thrust increases and reaches the maximum when heaving is still in the middle of its first quarter. Due to this upstroke motion, it goes to a minimum. At $\frac{t}{T} = 0.5$, the wing tip starts to move down while the root is in the negative phase of the cycle. Due to the downstroke motion, the wing tip again forces the air flow down and forward, and eventually generates positive lift and thrust forces, hence, reaches their maximum. Based on these observations, it can be stated that the resonance helps the wing to achieve flight favouring deforming motion that consequently generate higher aerodynamic forces.

Focusing the analysis at $f_n = f = 14$Hz (resonant frequency from FSI ($f_{FSI}$)), all $\phi$s are in-phase and are much higher than other frequencies. The forces $C_L$ and $C_T$ achieve their maximum at 14Hz. Also, $C_T$

https://doi.org/10.1017/aer.2022.71 Published online by Cambridge University Press

continues to increase after the maximum deflection. It can be seen in Fig. 12, as there are no bending and twisting near $t/T = 0.25$, the thrust $C_T$ also follow to a minimum at $t/T = 0.3$. As $\phi_b$ and $\phi_t$ progressively attain their maximum deflection in phase, the thrust $C_T$ correspondingly increases from the period $0.3 < t/T < 0.5$, and it appears to lag behind deflection slightly before reaching its maximum about $t/T = 0.6$.

### *3.4 Flow fields vs thrust*

To further understand the cause of the increased $C_T$ at $f_n$, Fig. 13 presents snapshots of the flow fields as thrust develops from minimum $C_T$ at four instances of $t/T = 0.200, 0.209, 0.215, 0.218$. The vorticity magnitude deduced via $\omega = \sqrt{\omega_x{}^2 + \omega_y{}^2 + \omega_z{}^2} = 30s^{-1}$ is shown in a light shade of grey, enclosing the contour of $\omega = 100$/s in a dark shade of grey. The direction of the vortex is schematically shown with yellow arrows. The surface pressure of the wing is represented in coloured contours. The velocity field (right) is shown at 80% chord about the $yz$ plane, while the wing is shown in amber. In Fig. 13(a), there is no pressure developed as the wing begins to flap into the page of the 3D view (i.e. flapping from left to right in the 2D velocity field view). However, a large vortex ring is formed combining the LE and TE vortices joining at the wing tip. This ring circulates the flow in the direction of the curved yellow arrows and acts onto the surface of the wing. The velocity field shows that the wake field pushes the wing in the lateral direction from left to right as well as the vertical direction in the 2D view. This is because the wing is projected in both directions due to the wing twist. The vertical direction is responsible for the thrust. The force is supported by the high-speed flow found in Fig.13(a) made possible and encased within the vortices above and below. The stream is analogously in the motion of plates in Ref.(48). As the wing flaps further into the page in Fig. 13(b), the vortex ring begins to detach from the surface near the 80% chord. The effect of the velocity field on the wing is reduced. By Fig. 13(c), the vortex ring separation leaves a hole for the flow to pass through from above to below, changing the general direction of recirculated flow behind towards a downward direction (see yellow arrow). The effect of this flow on the thrust diminishes, however, the pressure begins to accumulate near the tip as the deflections and wing movement slow down, and stop moving from left to right in the 2D view. It is this pressure acting on the wing that continues to push laterally, providing the lift, and a component of which is vertical, providing the thrust. By Fig. 13(d), the thrust reaches maximum. Note that the maximum surface pressure of the wing is also reached, and is the most substantial near 80% span. Figure 14 is a timeline of the event. Labels from (a) to (d) correspond to the instances in Fig. 13. It depicts, from the beginning of the stroke cycle to the end, how thrust as well as lift are developed. In summary, $C_T$ develops in two stages, first from the high intensity wake flow, second from the pressure build up. Both of which are onto the xy projection of the wing due to twist, lending to the continual increase of upward thrust through this portion of the flapping cycle. The influence of both the velocity field and pressure field on the movement of the wing is similar to the effect on freely falling flexible plates [49].

Following the finding of the flow field at maximum thrust at $f_n$, the flow fields in Fig. 13(e) provide the 10 and 20Hz flapping of the HIW at the maximum $C_T$ of their cycle, respectively. In comparison to the similar instant of maximum $C_T$ at $f_n$ of 14Hz in Fig. 13(d), both the size of vortices outlined and the pressure magnitudes are considerably smaller. This leads to the reduction in recirculating flow and the distributed force over the surface of the wing, such that the $C_T$ produced in Fig. 12 by the same wing is also significantly lower. Irregular formation of vortices at the midspan of the LE and the non-uniformity of the vortex rollup at the tip are observed. This leads to the abrupt changes of $C_T$ and $C_L$ in Fig. 12.

### *3.5 Experimental results*

We have performed modal testing of HIW model using a modal shaker. The fundamental natural frequencies are obtained by recording the tip displacements using a laser displacement sensor and performing FFT of the measured displacement data. The results are reported in Fig. 15(a). The first three fundamental natural frequencies of the wing are 14.88, 71.02 and 112.6Hz. The first experimental $f_n$ ($f_{\text{Experiment}}$) of

https://doi.org/10.1017/aer.2022.71 Published online by Cambridge University Press

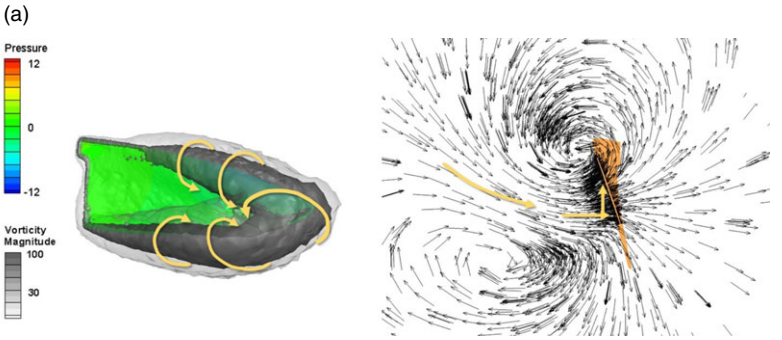


Flapping at 14 Hz at instance $t/T = 0.3$.

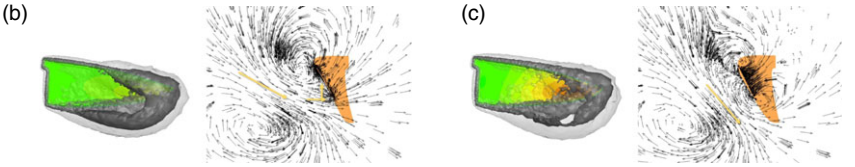


Flapping at 14 Hz at instance $t/T = 0.4$. Flapping at 14 Hz at instance $t/T = 0.5$.

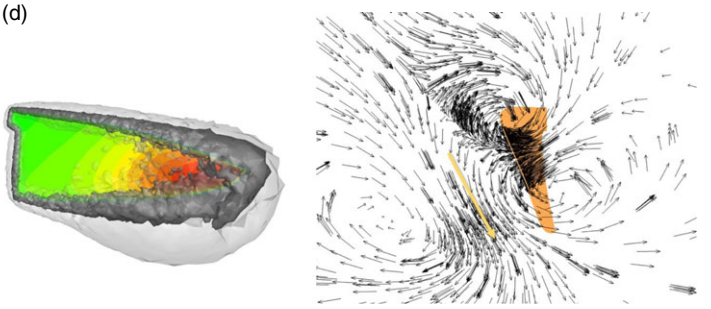


Flapping at 14 Hz at instance $t/T = 0.6$.

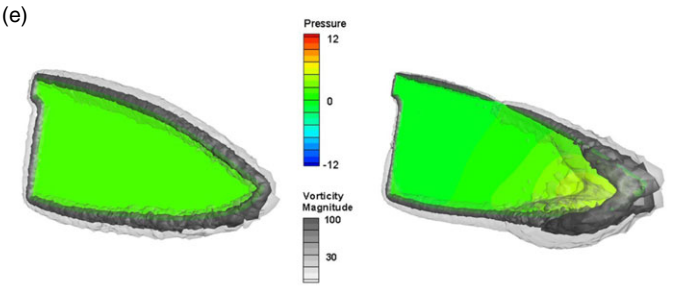


Flapping at 10Hz (left) and 20Hz (right) at respective maximum $C_T$.

***Figure 13.*** *(a-d) Flow fields p, ω and $v_x$ of HIW flapping at 14Hz corresponding to Fig. 12(d, e & f). Yellow arrows highlight the direction of flow. (e) Flow fields p and ω of HIW flapping at 10Hz and 20Hz.*

https://doi.org/10.1017/aer.2022.71 Published online by Cambridge University Press

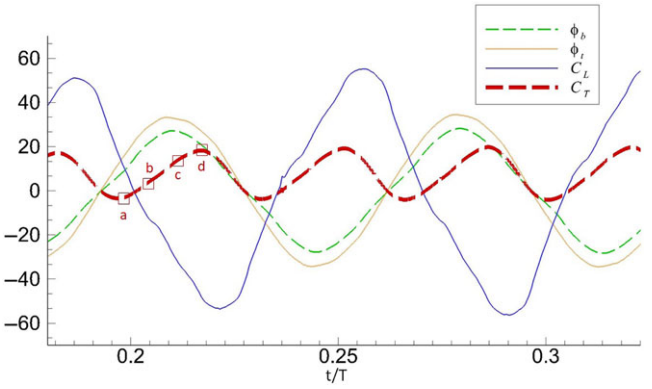


***Figure 14.*** *A timeline of two heaving cycles depicting the development of lift $C_L$ and thrust $C_T$. The labels a – d correspond to the figures in Fig. 13.*

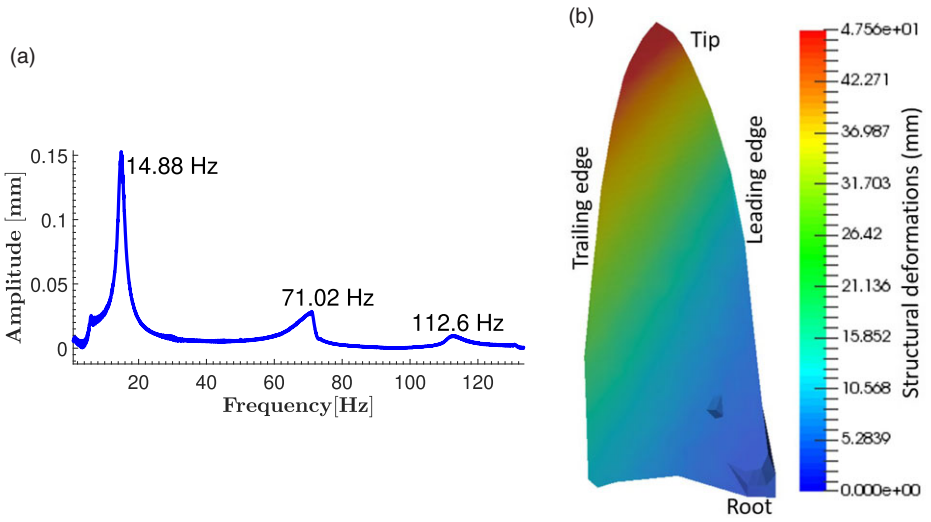


***Figure 15.*** *Experimental results, (a) natural frequencies, (b) wing deformations.*

HIW is close to the characteristic frequency of its natural counterpart, i.e. $f_{\text{Greenewalt}}$ (14.38Hz obtained using the Greenewalt relation given by Equation (1)), $f_{\text{Structure}}$ ($f_n$ from finite element modal analysis), $f_{\text{FSI}}$ ($f_n$ from FSI simulations). The comparison of these frequencies is shown in Table 4. This agreement validates the computational and analytical characteristic frequencies of the wing and further indicates that the present study is a successful step towards the biomimicking of hummingbird wings.

The physical models of HIW are attached to the heaving mechanism for structural motion measurement. The frequency of heaving is maintained at the experimental resonant frequency. The deforming shape of the wing is measured using an in-house 3D DIC-based non-contact motion measurement technique (see Fig. 7). The wing motion is recorded using the two synchronised high-speed cameras at 1,000fps. Only one wing's motion is considered, assuming the symmetric motion on the other wing. The recorded images are correlated to find the full-field displacements and generate complete deforming shape of the wing. The wing deformations from experiments are shown in Fig. 15(b). It can be seen that the physical wing model also generate a bending-twisting deforming shape which is

https://doi.org/10.1017/aer.2022.71 Published online by Cambridge University Press

***Table 4.*** *Comparison of Greenewalt, computational and experimental frequencies*

| $f_{\text{Greenewalt}}$ | $f_{\text{Structure}}$ | $f_{\text{FSI}}$ | $f_{\text{Experiment}}$ |
|---|---|---|---|
| 14.38Hz | 14.69Hz | 14Hz | 14.88Hz |

similar to computational results (see Fig. 8(a)). This validates and supports the structural deformation characteristics of the HIW model.

## 4.0 Conclusions

The present study was aimed towards realising the role of the flexibility and resonance in the deformation mechanism and aerodynamic performance of a hummingbird-inspired flapping wing under heaving excitation. In studying the role of flexibility, an aeroelastic flapping wing capable of producing bending-twisting deformations is designed by taking inspiration from hummingbirds. To study the role of resonance, the same wing design is analysed at off and on of its fundamental mode resonant frequency. Both types of investigations on the designed hummingbird-inspired wing (HIW) are carried out with the help of the computational FSI simulations. Novel materials were employed to model as well as physically realise the designed wing. The dynamics of the wing was deduced and validated through 3D digital image correlation-based non-contact motion measurements on a physical model of HIW. The physical wing prototype was realised by developing CNTs/PP nanocomposite films and using them with the commercially available CF/E composite sheets. In addition to that, a heaving mechanism was developed to excite the wings at different frequencies for obtaining the characteristic natural frequency, and measure the corresponding deforming motion of the wing at resonance.

Through the analysis of flexibility, it is shown that bending and twisting deformations are critical in enhancing the aerodynamic performance of flapping wings. It has been observed that lift and thrust are strongly related to wing deformations. In particular, the twisting of a wing allows the flow to affect the wing in the thrust direction in two ways. The first is from the recirculating wake onto the back of the wing; the second is the pressure accumulated as the wing and its deformation traverse in the reverse direction against the flow. As a result, the biomimetic hummingbird wing with large wing deflections receives a significant increase in thrust. This finding provides the missing link between the large deflections at resonance and its aerodynamic efficiency.

Compared to off-resonant frequencies, vorticity and pressures are substantially higher for the wing at resonance. This frequency is found to be at 14Hz and closely agrees with the empirically established value of 14.38Hz. The bending and twisting deformations of the wing are obtained experimentally and are in good agreement with the computation, which supports the FSI simulations performed in the present study.

The study finds that wing flexibility and resonance enhance the aerodynamic performance. More importantly, analysis from this work successfully resolves the FSI mechanisms that lead to the enhancement. These results and the physical biomimetic HIW fabrication are useful towards the development of efficient flapping wing micro aerial vehicles. It can be stated that the wing flexibility as well as the resonant excitation should be considered while designing a flapping aerial vehicle. Proper distribution of stiffness in the wing using realistic materials can help in generating desired wing deformations and frequency of flapping for enhancing the aerodynamic efficiency. The characteristic frequency of the flapping vehicle models should be determined before using them in real applications.

**Acknowledgements.** The authors thank Dr. Sudhir Kamle, Dr. Rakesh Kumar and Dr. G.M. Kamath for their valuable suggestions and support towards the present study. The technical support from Mr. Swapnil Shandliya, Mr. Vivek Khare, Mr. Lavendra Singh and Mr. C.P. Sharma during experimental work is highly appreciated. The financial support for the present study was provided by Indian Institute of Technology Kanpur, India and Chaoyang University of Technology, Taiwan.

## References


[1] Warrick, D.R., Tobalske, B.W. and Powers, D.R. Aerodynamics of the hovering hummingbird, *Nature*, 2005, **435**, (7045), pp 1094–1097.

[2] Elimelech, Y. and Ellington, C.P. Analysis of the transitional flow field over a fixed hummingbird wing, *J. Exp. Biol.*, 2013, **216**, (2), pp 303–318.

[3] Altshuler, D.L., Dudley, R. and Ellington, C.P. Aerodynamic forces of revolving hummingbird wings and wing models, *J. Zool.*, 2004, **264**, (4), pp 327–332.

[4] Kruyt, J.W., QuicazÁn-Rubio, E.M., van Heijst, G.F., Altshuler, D.L. and Lentink, D. Hummingbird wing efficacy depends on aspect ratio and compares with helicopter rotors, *J. R. Soc. Interface*, 2014, **11**, (99), p. 20140585.

[5] Greenewalt, C.H. *Hummingbirds*, Doubleday, 1960, New York.

[6] Greenewalt, C.H. The flight of birds: The significant dimensions, their departure from the requirements for dimensional similarity, and the effect on flight aerodynamics of that departure. *Trans. Am. Philos. Soc.*, 1975, **65**, (4), pp 1–67.

[7] Wells, D.J. Muscle performance in hovering hummingbirds, *J. Exp. Biol.*, 1993, **178**, (1), pp 39–57.

[8] Maeda, M., Nakata, T., Kitamura, I., Tanaka, H. and Liu, H. Quantifying the dynamic wing morphing of hovering hummingbird, *R. Soc. Open Sci.*, 2017, **4**, (9), p 170307.

[9] Tobalske, B.W., Warrick, D.R., Clark, C.J., Powers, D.R., Hedrick, T.L., Hyder, G.A. and Biewener, A.A. Three-dimensional kinematics of hummingbird flight, *J. Exp. Biol.*, 2007, **210**, (13), pp 2368–2382.

[10] Ingersoll, R. and Lentink, D. How the hummingbird wingbeat is tuned for efficient hovering, *J. Exp. Biol.*, 2018, **221**, (178228) DOI: 10.1242/jeb.178228.

[11] Greenewalt, C.H. The wings of insects and birds as mechanical oscillators, *Proc. Am. Philos. Soc.*, 1960, **104**, (6), pp 605–611.

[12] Jafferis, N.T., Graule, M.A. and Wood, R.J. Non-linear resonance modeling and system design improvements for underactuated flapping-wing vehicles, 2016 IEEE International Conference on Robotics and Automation, IEEE, pp 3234–3241.

[13] Zhang, J. and Deng, X. Resonance principle for the design of flapping wing micro air vehicles, *IEEE Trans. Robot.*, 2017, **33**, (1), pp 183–197.

[14] Raney, D.L. and Slominski, E.C. Mechanization and control concepts for biologically inspired micro air vehicles, *J. Aircraft*, 2004, **41**, (6), pp 1257–1265.

[15] Chen, J.S., Chen, J.Y. and Chou, Y.F. On the natural frequencies and mode shapes of dragonfly wings, *J. Sound Vib.*, 2008, **313**, (3–5), pp 643–654.

[16] Combes, S.A. and Daniel, T.L. Into thin air: Contributions of aerodynamic and inertial-elastic forces to wing bending in the hawkmoth Manduca sexta, *J. Exp. Biol.*, 2003, **206**, (17), pp 2999–3006.

[17] Masoud, H. and Alexeev, A. Resonance of flexible flapping wings at low Reynolds number, *Phys. Rev. E*, 2010, **81**, (5), p 056304.

[18] Tobing, S., Young, J. and Lai, J.C.S. Effects of wing flexibility on bumblebee propulsion, *J. Fluids Struct.*, 2017, **68**, pp 141–157.

[19] Young, J., Walker, S.M., Bomphrey, R.J., Taylor, G.K. and Thomas, A.L. Details of insect wing design and deformation enhance aerodynamic function and flight efficiency, *Science*, 2009, **325**, (5947), pp 1549–1552.

[20] Frampton, K.D., Goldfarb, M., Monopoli, D. and Cveticanin, D. Passive aeroelastic tailoring for optimal flapping wings, *Progr. Astronaut. Aeronaut.*, 2001, **195**, pp 473–482.

[21] Heathcote, S. and Gursul, I. Flexible flapping airfoil propulsion at low Reynolds numbers, *AIAA J.*, 2007, **45**, (5), pp 1066–1079.

[22] Lin, T., Xia, W. and Hu, S. Effect of chordwise deformation on propulsive performance of flapping wings in forward flight, *Aeronaut. J.*, 2021, **125**, (1284), pp 430–451.

[23] DeLaurier, J.D. The development of an efficient ornithopter wing, *Aeronaut. J.*, 1993, **97**, (965), pp 153–162.

[24] Mazaheri, K. and Ebrahimi, A. Experimental study on interaction of aerodynamics with flexible wings of flapping vehicles in hovering and cruise flight, *Arch. Appl. Mech.*, 2010, **80**, (11), pp 1255–1269.

[25] Chimakurthi, S.K., Tang, J., Palacios, R., Cesnik, C.E.S. and Shyy, W. Computational aeroelasticity framework for analyzing flapping wing micro air vehicles, *AIAA J.*, 2009, **47**, (8), pp 1865–1878.

[26] Ryu, Y., Chang, J.W., Chung, J. and Kim, D.H. Experimental investigation of flexible hawkmoth-like wings on the wing-wake interaction in hovering flight, *J. Bionic Eng.*, 2018, **15**, (1), pp 139–153.

[27] Aono, H., Chimakurthi, S.K., Cesnik, C.E.S., Liu, H. and Shyy, W. Computational modeling of spanwise flexibility effects on flapping wing aerodynamics, 47th AIAA Aerospace Sciences Meeting including the New Horizons Forum and Aerospace Exposition, p 1270.

[28] Tang, J., Viieru, D. and Shyy, W. A study of aerodynamics of low Reynolds number flexible airfoils, 37th AIAA Fluid Dynamics Conference and Exhibit, p 4212.

[29] Kumar, D., Goyal, T., Kamle, S., Mohite, P. and Lau, E. Realisation and testing of novel fully articulated bird-inspired flapping wings for efficient and agile UAVs, *Aeronaut. J.* 2021, **125**, (1294), pp 2114–2148.

[30] Senda, K., Obara, T., Kitamura, M., Yokoyama, N., Hirai, N. and Iima, M. Effects of structural flexibility of wings in flapping flight of butterfly, *Bioinspiration Biomimetics*, 2012, **7**, (2), p 025002.

[31] Kumar, D., Mohite, P.M. and Kamle, S. Dragonfly inspired nanocomposite flapping wing for micro air vehicles, *J. Bionic Eng.*, 2019, **16**, (5), pp 894–903.

[32] Kumar, D. and Shandilya, S. A bioinspired MAV with nanocomposite wings and flexure joints: design and structural dynamic analysis, *Int. J. Appl. Sci. Eng.*, 2021, **18**, (2), pp 1–15.

[33] Bonser, R. and Purslow, P. The Young's modulus of feather keratin, *J. Exp. Biol.*, 1995, **198**, (4), pp 1029–1033.


https://doi.org/10.1017/aer.2022.71 Published online by Cambridge University Press

[34] Burton, R. *The World of the Hummingbird*, Firefly Books, 2001, New York.
[35] Kumar, V.S., Kumar, D., Goyal, T., Mohite, P.M. and Kamle, S. Development and application of PP-CNT composite for hummingbird inspired MAV flapping wings, International Micro Air Vehicle Conference and Competition, pp 180–187.
[36] Song, J., Luo, H. and Hedrick, T.L. Three-dimensional flow and lift characteristics of a hovering ruby-throated hummingbird, *J. R. Soc. Interface*, 2014, **11**, (98), p 20140541.
[37] Glück, M., Breuer, M., Durst, F., Halfmann, A. and Rank, E. Computation of fluid–structure interaction on lightweight structures, *J. Wind Eng. Ind. Aerodyn.*, 2001, **89**, (14–15), pp 1351–1368.
[38] Chimakurthi, S.K., Reuss, S., Tooley, M. and Scampoli, S. ANSYS Workbench System Coupling: A state-of-the-art computational framework for analyzing multiphysics problems, *Eng. Comput.*, 2018, **34**, (2), pp 385–411.
[39] Lee, J. and Lee, S. Fluid–structure interaction analysis on a flexible plate normal to a free stream at low Reynolds numbers, *J. Fluids Struct.*, 2012, **29**, pp 18–34.
[40] Tobing, S., Young, J. and Lai, J.C.S. A numerical analysis of bumblebee propulsion, 31st AIAA Applied Aerodynamics Conference, p 3049.
[41] Kumar, D., Kamle, S., Mohite, P.M. and Kamath, G.M. A novel real-time DIC-FPGA-based measurement method for dynamic testing of light and flexible structures, *Meas. Sci. Technol.*, 2019, **30**, (4), p 045903.
[42] Ha, N.S., Truong, Q.T., Goo, N.S. and Park, H.C. Relationship between wingbeat frequency and resonant frequency of the wing in insects, *Bioinspiration Biomimetics*, 2013, **8**, (4), p 046008.
[43] Ramananarivo, S., Godoy-Diana, R. and Thiria, B. Rather than resonance, flapping wing flyers may play on aerodynamics to improve performance, *Proc. Natl Acad. Sci.*, 2011, **108**, (15), pp 5964–5969.
[44] Yin, B. and Luo, H. Effect of wing inertia on hovering performance of flexible flapping wings, *Phys. Fluids*, 2010, **22**, (11), p 111902.
[45] Tian, F.B., Luo, H., Song, J. and Lu, X.Y. Force production and asymmetric deformation of a flexible flapping wing in forward flight, *J. Fluids Struct.*, 2013, **36**, pp 149–161.
[46] Shahzad, A., Tian, F.B., Young, J. and Lai, J.C.S. Effects of hawkmoth-like flexibility on the aerodynamic performance of flapping wings with different shapes and aspect ratios, *Phys. Fluids*, 2018, **30**, (9), p 091902.
[47] Shahzad, A., Tian, F.B., Young, J. and Lai, J.C.S. Effects of flexibility on the hovering performance of flapping wings with different shapes and aspect ratios, *J. Fluids Struct.*, 2018, **81**, pp 69–96.
[48] Wan, H., Dong, H. and Liang, Z. Vortex formation of freely falling plates, 50th AIAA Aerospace Sciences Meeting Including the New Horizons Forum and Aerospace Exposition, p 1079.
[49] Lau, E.M. and Huang, W.X. Variations of flight patterns for falling flexible plates, *Phys. Fluids*, 2021, **33**, (8), p 081904.

**Cite this article:** Kumar D., Singh G., Mohite P.M., Lau E.M. and Wang Y.-C. (2023). Role of flexibility on the aerodynamic performance of a resonating hummingbird-inspired wing. *The Aeronautical Journal*, **127**, 193–212. https://doi.org/10.1017/aer.2022.71